# Organ-specific metastases obtained by culturing colorectal cancer cells on tissue-specific decellularized scaffolds

| | |
|---|---|
| Supplementary Figure 1 | Decellularization of lung and liver tissues produces BMSs containing tissue specific signaling molecules. |
| Supplementary Figure 2 | The composition of extracellular matrix components differs between liver and lung BMSs. |
| Supplementary Figure 3 | Scanning electron micrographs of CRC119 cells spontaneously formed 3D engineered metastases when cultured on liver and lung BMSs. |
| Supplementary Figure 4 | Transmission electron micrographs of the engineered liver metastases. |
| Supplementary Figure 5 | Engineered metastases grow relatively slowly due to reduced proliferation rates. |
| Supplementary Figure 6 | Sequential gating strategy was used to identify EdU positive CRC cell subsets. |
| Supplementary Figure 7 | Representative histological images of HT-29, SW480, and Caco2 cells grown on plastic, collagen, Matrigel, liver BMSs and lung BMSs. |
| Supplementary Figure 8 | Engineered liver metastases and *in vivo* metastases demonstrate comparable gene signatures. |
| Supplementary Figure 9 | Engineered metastases demonstrate increased metastatic potential *in vivo*. |
| Supplementary Figure 10 | Photograph of liver metastases 45 days post direct hepatic or iv injection with SW480 cells isolated from plastic, liver BMSs, and lung BMSs. |
| Supplementary Figure 11 | Photograph of liver metastases 45 days post direct hepatic or iv injection with Caco2 cells isolated from plastic, liver BMSs, and lung BMSs. |
| Supplementary Figure 12 | Whole organ *ex vivo* bioluminescent imaging and histological analyses were used to confirm the presence of metastatic lesions identified based on whole animal bioluminescent images. |
| Supplementary Figure 13 | Characterization of the relative susceptibility to anoikis and invasive potential displayed by CRC cells grown on different culture substrata. |
| Supplementary Figure 14 | Hypoxic preconditioning does not increase the metastatic potential of HT-29 cells grown on plastic. |
| Supplementary Table 1 | Table summarizing the histological features identified in cultures produced by HT-29, SW480, and Caco2 when grown on plastic, collagen, Matrigel, liver BMSs and lung BMSs. |

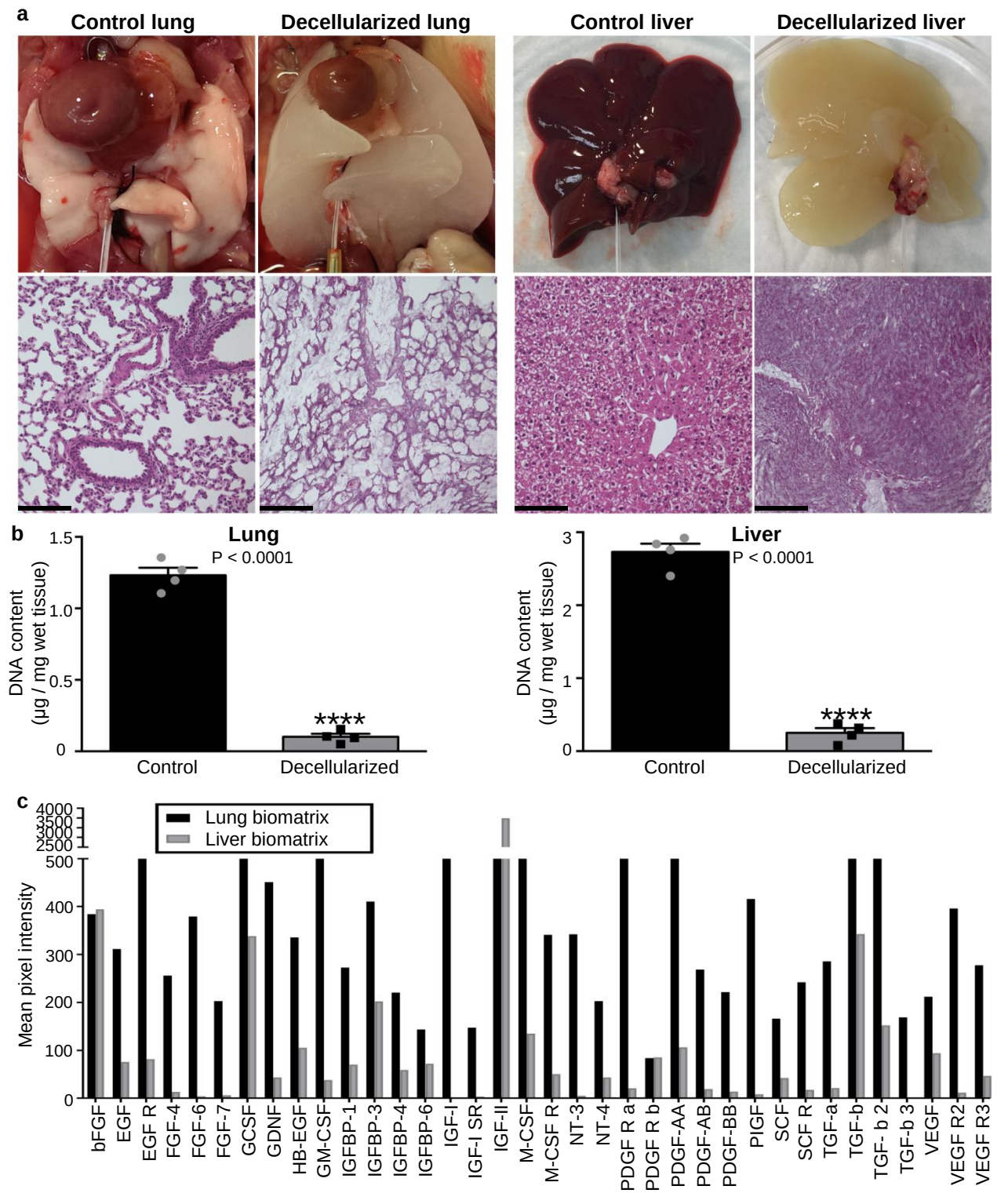


**Supplementary Figure 1:** Decellularization of lung and liver tissues produces BMSs containing tissue specific signaling molecules (a) Macroscopic and H&E images of lung (left) and liver (right) before and after decellularization. The experiment was repeated ten times. Scale bars, 130 µm. (b) Assessment of DNA content present in lungs and livers before and after decellularization (n=3 biological independent samples). Data represent mean ± S.E.M. Differences in DNA content were determined using two-sided t-test. (****$P < 0.0001$). (c) Analysis of growth factors and cytokines present in lung and liver BMSs (n=4). Mean pixel intensity values for signaling molecules present in liver BMSs were obtained from a previous publication[11].

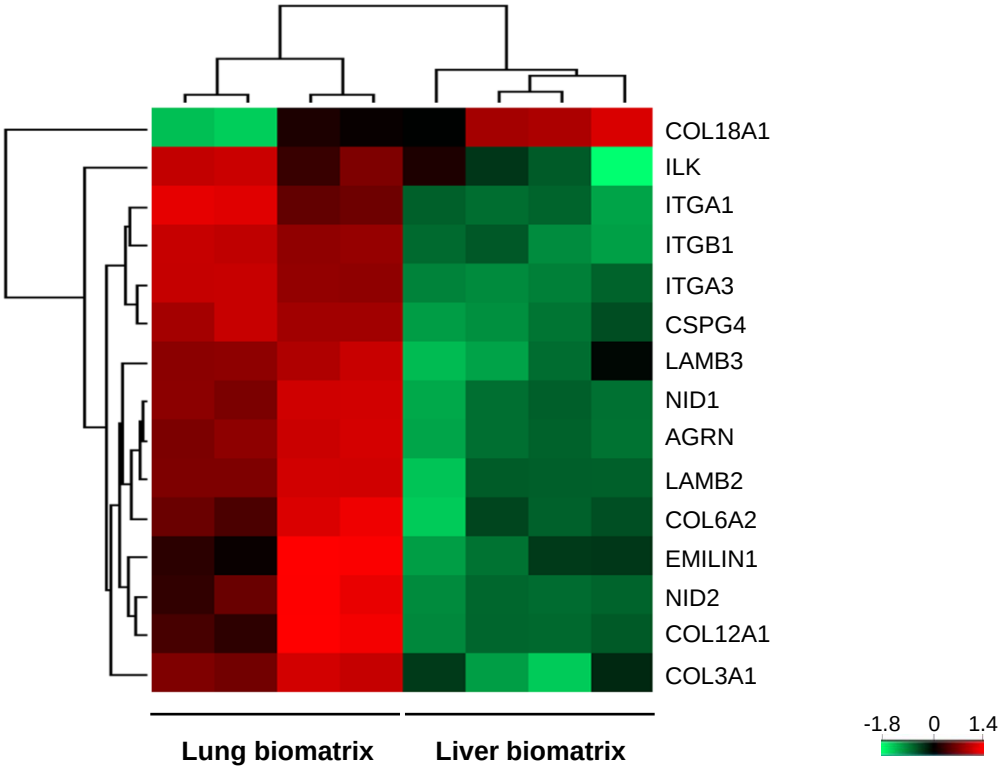


**Supplementary Figure 2:** The composition of extracellular matrix components differs between liver and lung BMSs. Heat map comparing the relative abundance of collagens, elastins, fibronectins, and lamins that are differentially expressed in liver and lung BMSs (n=4 biologically independent samples). Hierarchical clustering was performed using z-score normalized label-free quantification intensities.

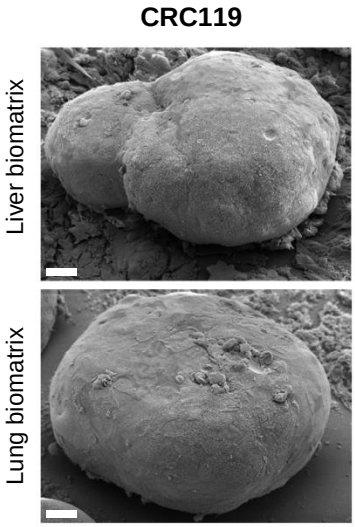


**Supplementary Figure 3:** Scanning electron micrographs of CRC119 cells spontaneously formed 3D engineered metastases when cultured on liver and lung BMSs. Experiments were repeated three times independently with similar results. Scale bars, 50 μm.

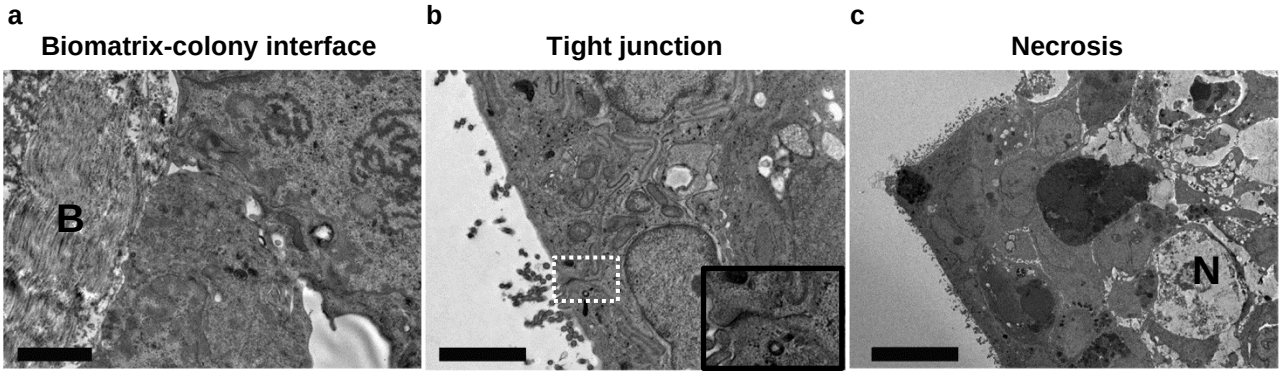


**Supplementary Figure 4:** Transmission electron micrographs of the engineered liver metastases depicting (a) the interface between the colony and the biomatrix scaffold, (b) tight junctions between cells, and (c) areas of necrosis. (a-b) Scale bars, 2 µm. (c) Scale bar, 10 µm. Biomatrix scaffold in the left panel is indicated by "B". A tight junction in the middle panel is indicated by a dotted box. A necrotic area in the right panel is indicated by "N". Experiments were repeated three times independently with similar results.

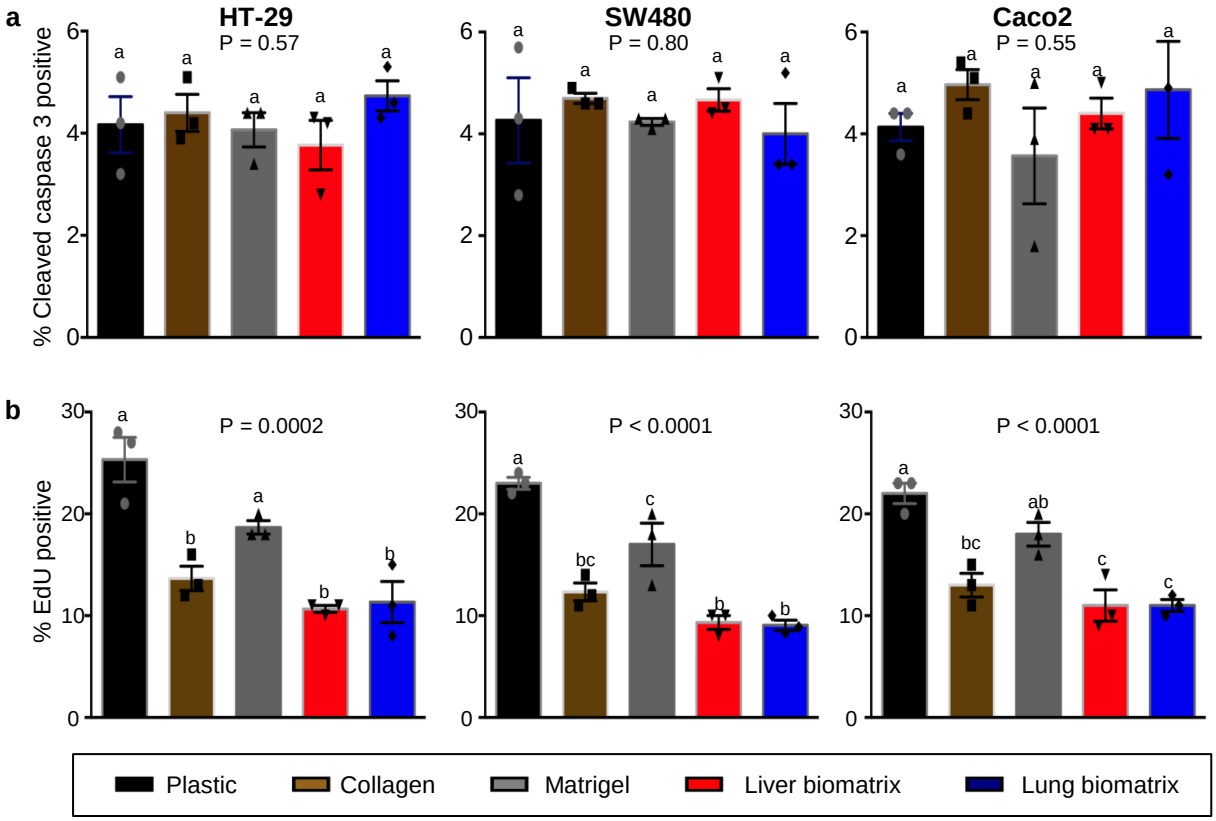


**Supplementary Figure 5:** Engineered metastases grow relatively slowly due to reduced proliferation rates. (a) Quantification of cells undergoing apoptosis, Cleaved Caspase 3 positive, in CRC cultures grown on plastic, collagen, Matrigel, liver BMSs, and lung BMSs using flow cytometry (n=3 biologically independent cell samples). (b) Quantification of the number of cells cultured on different substrata that underwent S-phase, EdU positive, over a four hour labeling period as assessed by flow cytometry (n=3 biologically independent cell samples). Data represent mean ± S.E.M. Differences in apoptosis and proliferation rate were assessed using a one-way ANOVA with Tukey's multiple comparison post-test. Statistical significance is indicated with letters above ($P < 0.05$) using. Groups that share the same letter are not significantly different.

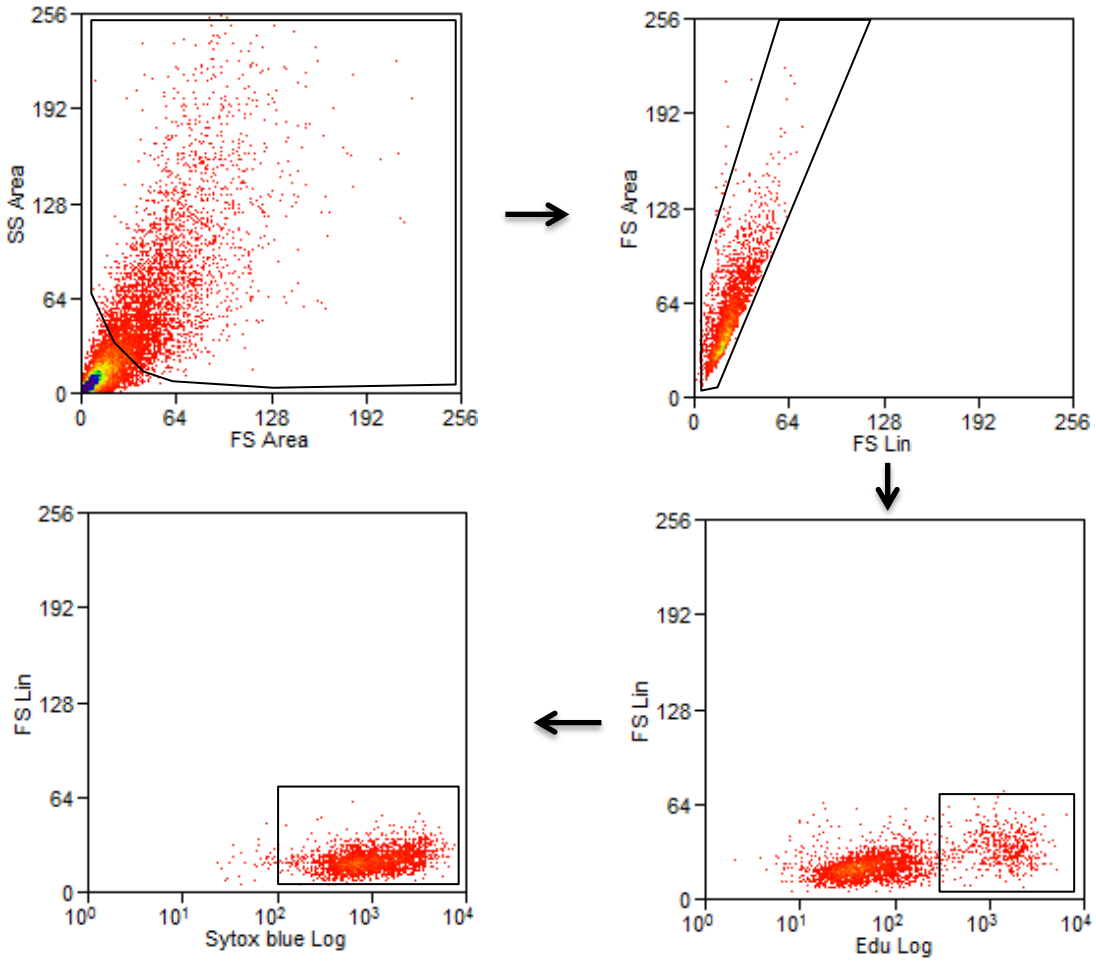


**Supplementary Figure 6:** Sequential gating strategy was used to identify EdU positive CRC cell subsets. The same flow cytometry gating strategy was also used for Cleaved Caspase 3 positive CRC cell subsets.

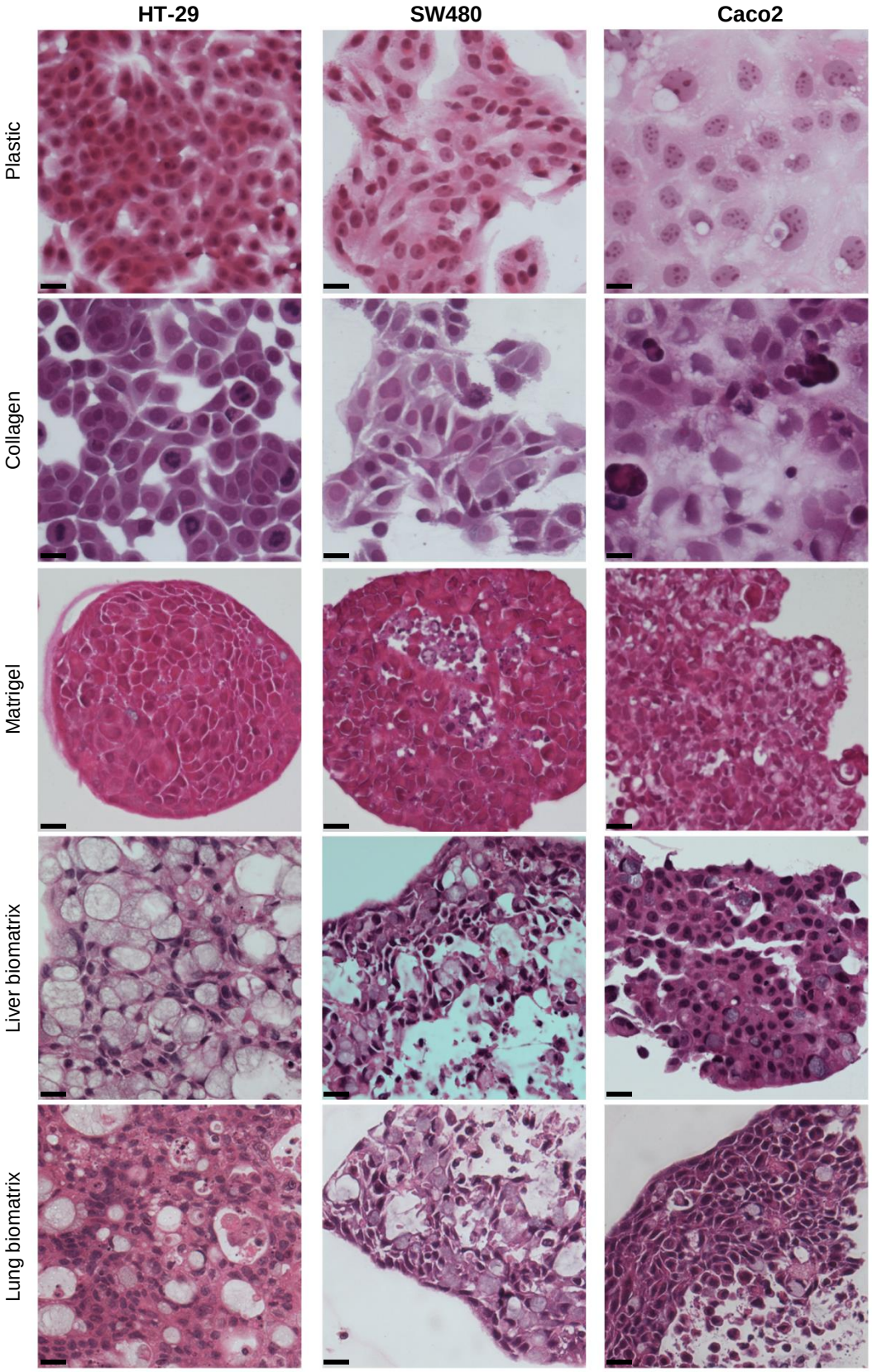


**Supplementary Figure 7:** Representative images of HT-29 (left), SW480 (middle), and Caco2 (right) cells grown on plastic, collagen, Matrigel, liver BMSs and lung BMSs. The experiment was repeated three times independently with similar results. Scale bars, 20 µm.

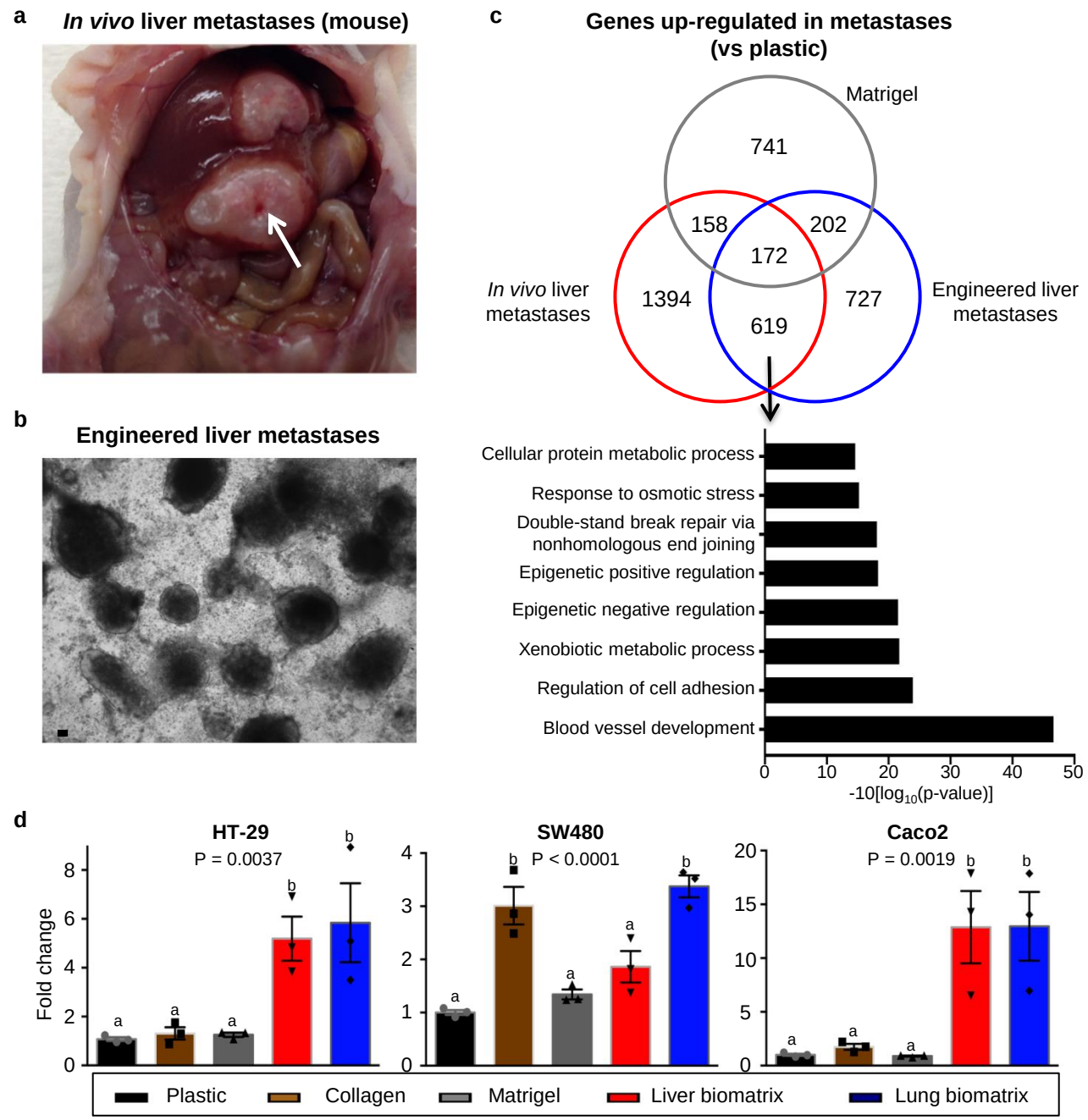


**Supplementary Figure 8:** Engineered liver metastases and *in vivo* metastases demonstrate comparable gene signatures (a) Global gene expression profiles of *In vivo* HT-29 liver metastases and (b) engineered liver metastases were assessed by microarray analysis (n=4 biological independent samples). Liver metastases in (a) is indicated by white arrow. The experiments was repeated three times independently with similar results. Scale bars, 100 µm. (c) Venn diagram depicting the number of genes up-regulated in Matrigel cultures, engineered metastases, and *in vivo* liver metastases when compared to cells grown on plastic. Gene ontology analysis reveals that many commonly up-regulated genes are associated with angiogenesis, cellular adhesion, and drug metabolism (d) *Timp1* gene expression in HT-29, SW480, and Caco2 cells grown on plastic, collagen, Matrigel, liver and lung BMSs as assessed by real-time qPCR (n=4 biologically independent samples). Data represent mean ± S.E.M. Differences in *Timp1* expression were determined using a one-way ANOVA with Tukey's multiple comparison post-test. Statistical significance is indicated with letters above ($P < 0.05$). Groups that share the same letter are not significantly different.

**a**

| Cell source for injection | Lung metastases | Liver metastases |
|---|---|---|
| Plastic | 0/10 | 0/10 |
| Collagen | 0/10 (p=1) | 0/10 (p=1) |
| Matrigel | 0/10 (p=1) | 1/10 (p=1) |
| Liver biomatrix | 0/10 (p=1) | 7/10 (p=0.03) |
| Lung biomatrix | 0/10 (p=1) | 4/10 (p=0.087) |

**c**

| Cell source for injection | Lung metastases | Liver metastases |
|---|---|---|
| Plastic | 2/10 | 0/10 |
| Collagen | 0/10 (p=0.47) | 0/10 (p=1) |
| Matrigel | 1/10 (p=1) | 0/10 (p=1) |
| Liver biomatrix | 8/10 (p=0.02) | 5/10 (p=0.03) |
| Lung biomatrix | 7/10 (p=0.069) | 2/10 (p=0.47) |

**b**

| Cell source for injection | Lung metastases | Liver metastases |
|---|---|---|
| Plastic | 0/10 | 1/10 |
| Collagen | 0/10 (p=1) | 2/10 (p=1) |
| Matrigel | 0/10 (p=1) | 3/10 (p=0.58) |
| Liver biomatrix | 0/10 (p=1) | 7/10 (p=0.019) |
| Lung biomatrix | 0/10 (p=1) | 5/10 (p=0.14) |

**d**

| Cell source for injection | Lung metastases | Liver metastases |
|---|---|---|
| Plastic | 0/10 | 0/10 |
| Collagen | 1/10 (p=1) | 0/10 (p=1) |
| Matrigel | 0/10 (p=1) | 0/10 (p=1) |
| Liver biomatrix | 6/10 (p=0.01) | 4/10 (p=0.08) |
| Lung biomatrix | 7/10 (p=0.003) | 0/10 (p=1) |

**Supplementary Figure 9:** Engineered metastases demonstrate increased metastatic potential *in vivo*. Table summarizing the number of animals that developed liver and lung metastases post (a,b) direct hepatic injection or (c,d) tail vein injection of CRC cells (n=10 biologically independent animals per group). (a,c) HT-29-luc2 cells and (b,d) CRC119 cells were isolated from plastic, collagen, Matrigel, liver BMSs, and lung BMSs. The experiments was repeated twice and the results were pooled. P values for two-sided Fisher's exact test comparison of tumor incidence in mice injected with cells grown on different substrata to that in control ("Plastic") group are given in parentheses.

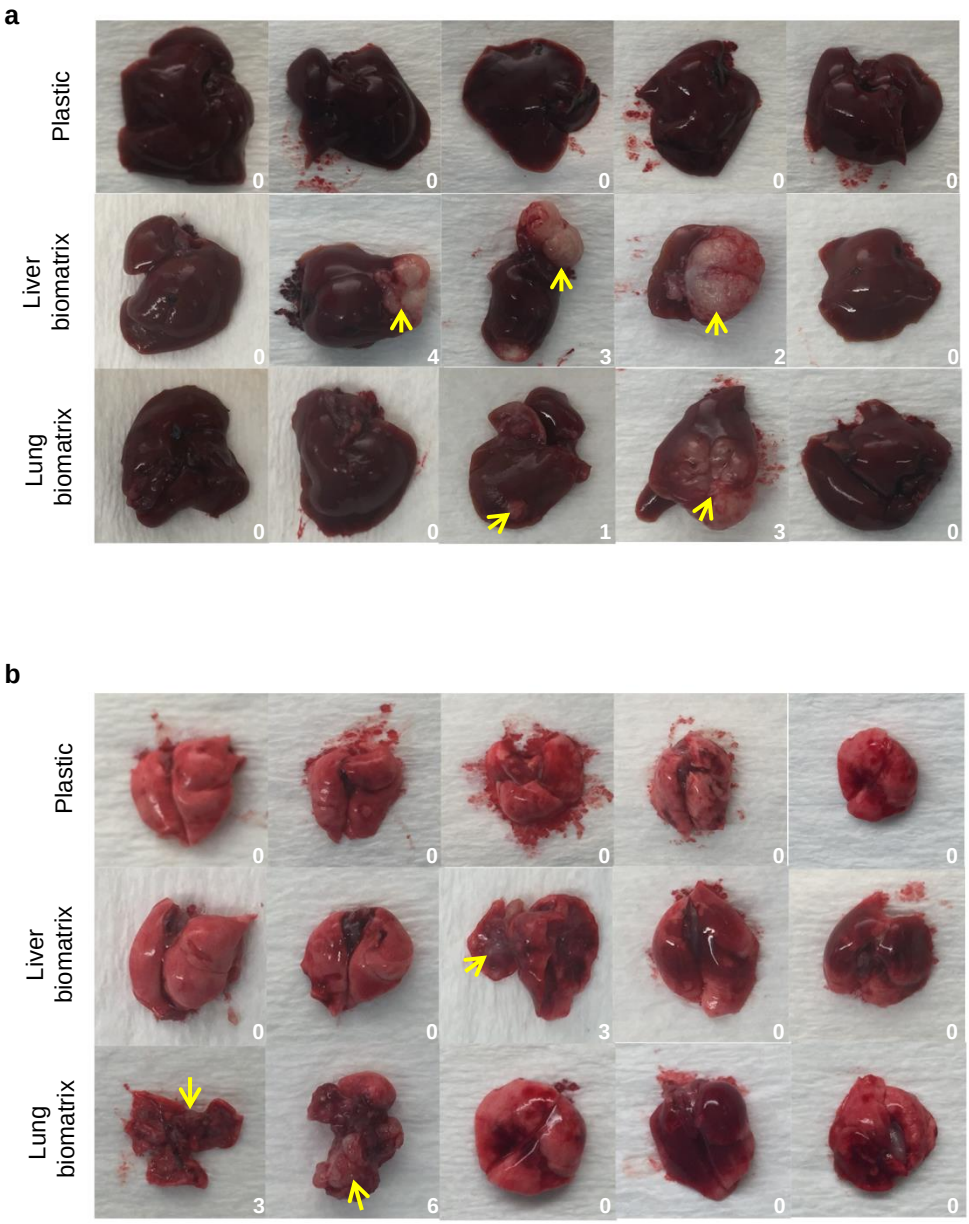


**Supplementary Figure 10:** (a) Photograph of liver metastases (indicated by yellow arrows) 45 days post direct hepatic injection with SW480 cells isolated from plastic, liver BMSs, and lung BMSs. (b) Photograph of pulmonary metastases (indicated by yellow arrows) 45 days post tail vein injection with SW480 cells isolated from plastic, liver BMSs, and lung BMSs. The number of metastatic nodes was indicated in the bottom right corner of each photograph.

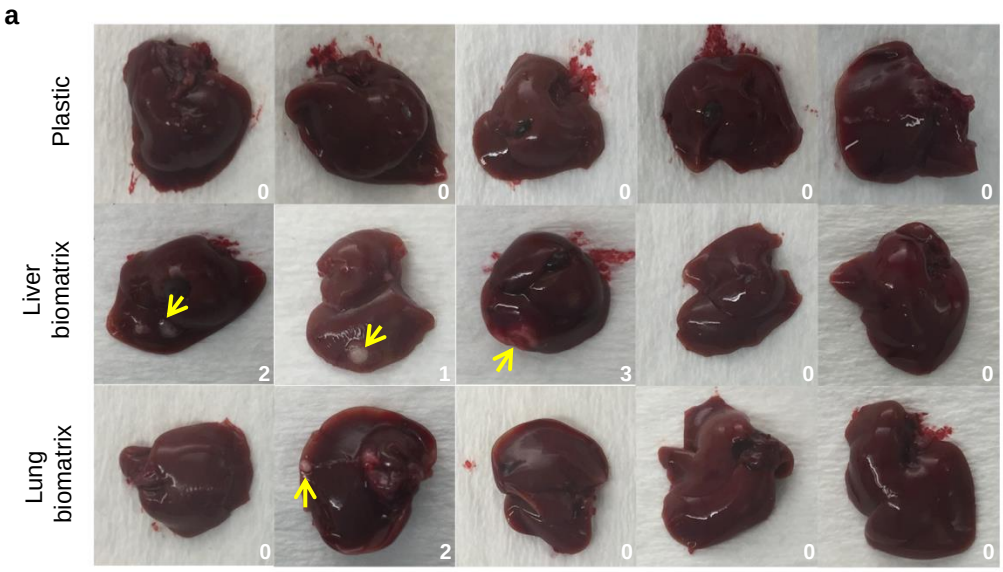


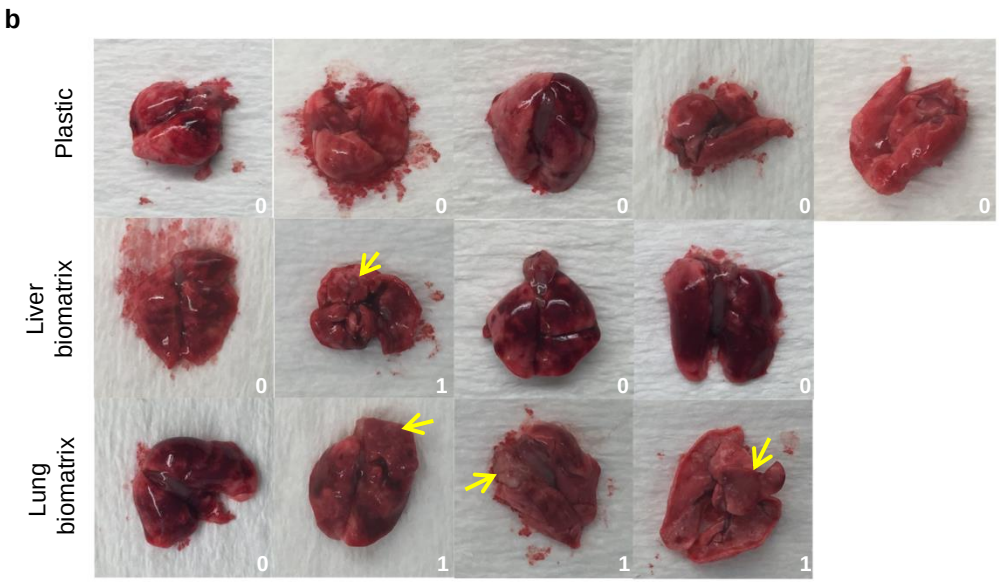


**Supplementary Figure 11:** (a) Photograph of liver metastases (indicated by yellow arrows) 45 days post direct hepatic injection with Caco2 cells isolated from plastic, liver BMSs, and lung BMSs. (b) Photograph of pulmonary metastases (indicated by yellow arrows) 45 days post tail vein injection with Caco2 cells isolated from plastic, liver BMSs, and lung BMSs. The initial animal numbers for each group was 5 but one mouse was unintentionally culled. The number of metastatic nodes was indicated in the bottom right corner of each photograph.

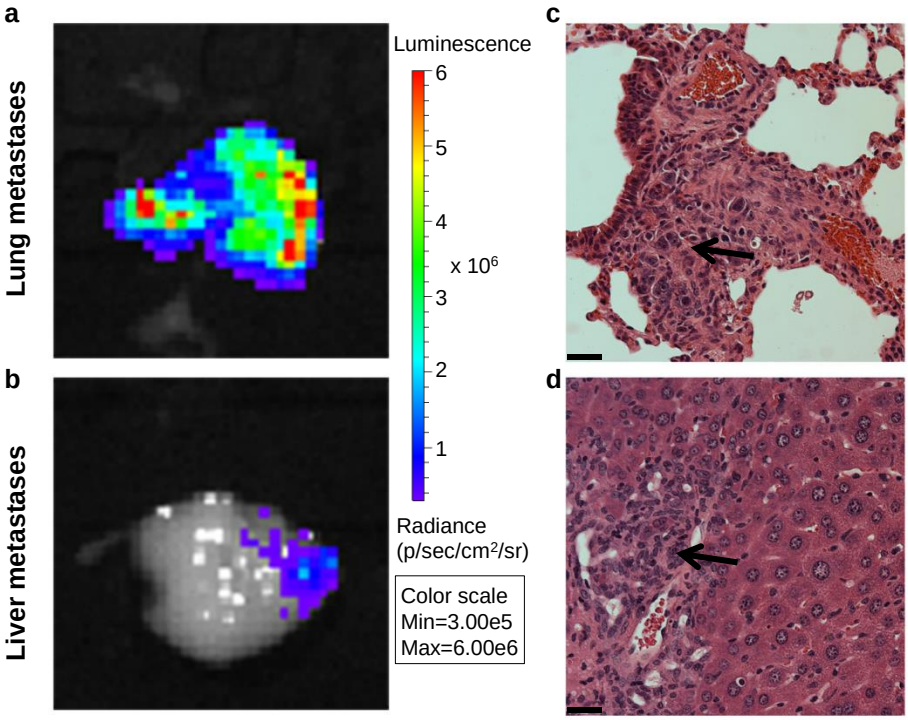


**Supplementary Figure 12:** Whole organ *ex vivo* bioluminescent imaging and histological analyses were used to confirm the presence of metastatic lesions identified based on whole animal bioluminescent images following tail vein injection (a) or direct hepatic injection (b) of HT29-luc2 cells. Representative liver and lung metastases identified by histology are indicated by an arrow. The experiments was repeated five times independently with similar results. Scale bars, 20 µm.

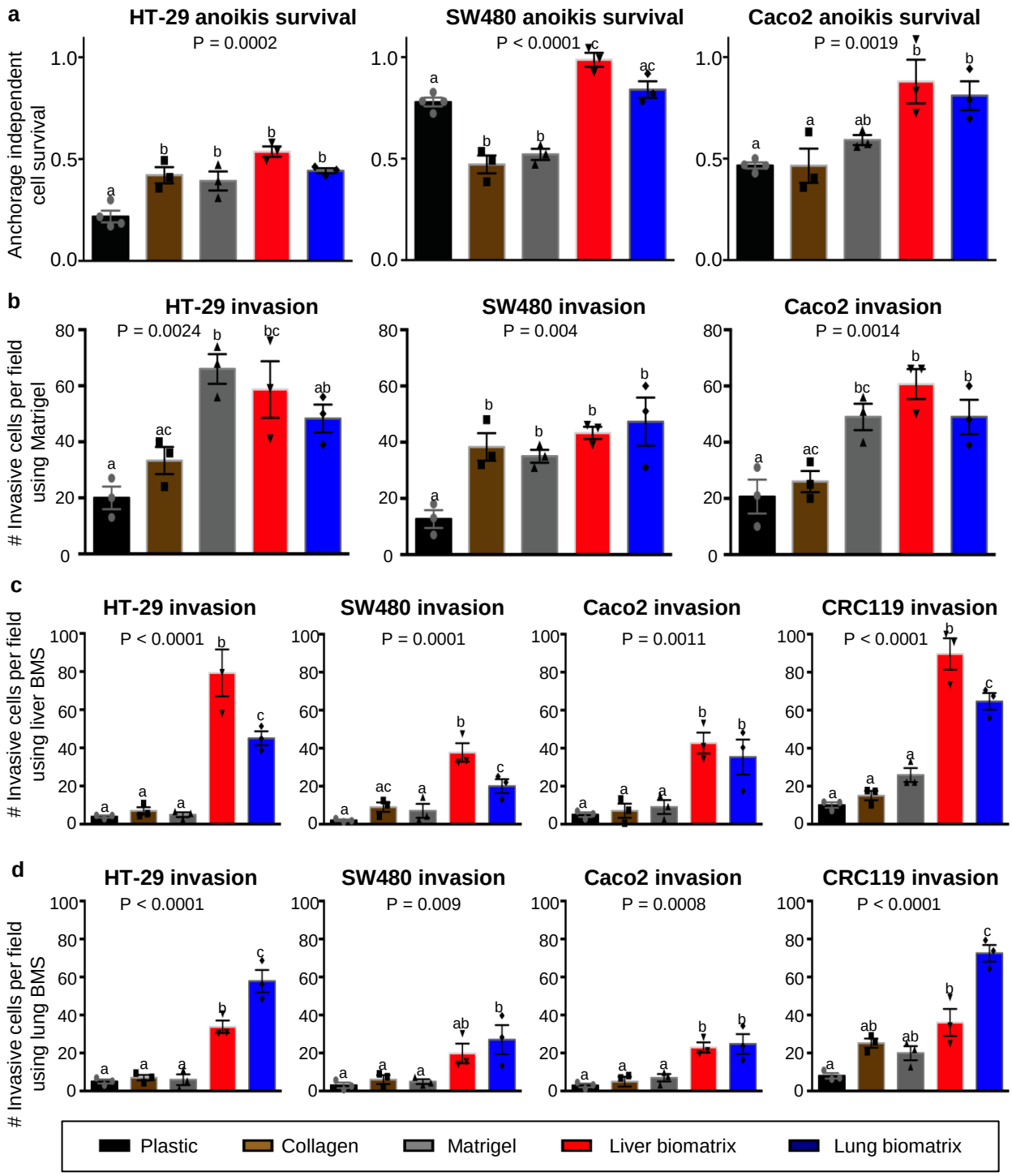


**Supplementary Figure 13:** Characterization of the relative susceptibility to anoikis and invasive potential displayed by CRC cells grown on different culture substrata. (a) Relative resistance of HT-29, SW480, and Caco2 cells grown on plastic, collagen, Matrigel, liver BMSs, and lung BMSs to undergoing anoikis following culture on hydrogel-coated plates (n=3 biologically independent experiments). (b) Invasion potential of CRC cells grown on different substrata as determined using a Matrigel-coated transwell invasion assay (n=3 biologically independent experiments). Further, invasion potential of CRC cells (HT-29, SW480, Caco2, and CRC119) grown on different substrata as determined using (c) liver or (d) lung BMSs as invasion barriers. (n=3 biologically independent experiments). Data represent mean ± S.E.M. Differences in survival and invasion were determined using a one way ANOVA with Tukey's multiple comparison post-test. Statistical significance is indicated with letters above ($P < 0.05$). Groups that share the same letter are not significantly different.

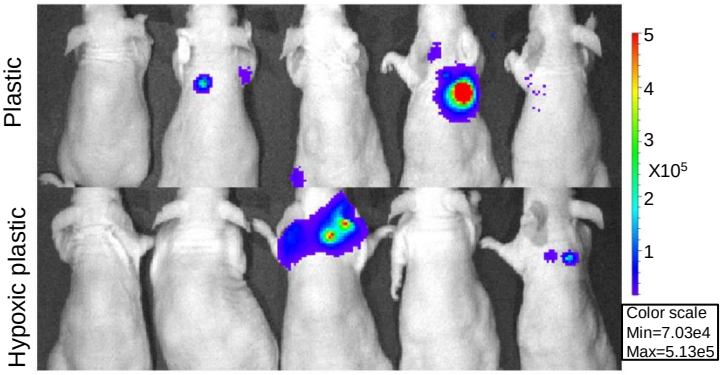


**Supplementary Figure 14:** Hypoxic preconditioning does not increase the metastatic potential of HT-29 cells grown on plastic. Bioluminescence images of animals 30 days post tail vein injection of HT-29-luc2 cells cultured under normal and hypoxic conditions, showing the same number (2/5) of animals that developed lung metastases. No animals (0/5) in either group developed liver metastases.

**Supplementary Table 1:** Table summarizing the histological features identified in cultures produced by HT-29, SW480, and Caco2 when grown on plastic, collagen, Matrigel, liver BMSs and lung BMSs.

| | | Signet ring cells | Bizarre mitotic figures | Necrotic debris | Pleomorphism | Multinucleated cells |
|---|---|---|---|---|---|---|
| **HT-29** | Plastic | | | | | |
| | Collagen | | X | | | X |
| | Matrigel | | X | | | X |
| | Liver biomatrix | X | X | X | X | X |
| | Lung biomatrix | X | | X | X | X |
| **SW480** | Plastic | | | | | X |
| | Collagen | | | | | X |
| | Matrigel | | | | | X |
| | Liver biomatrix | X | X | X | X | X |
| | Lung biomatrix | X | | X | X | X |
| **Caco2** | Plastic | | X | | X | |
| | Collagen | | X | | X | X |
| | Matrigel | | X | | X | |
| | Liver biomatrix | X | X | X | | X |
| | Lung biomatrix | X | X | X | | X |